Molecular Vision 2016; 22:1291-1308 <http://www.molvis.org/molvis/v22/1291>
Received 1 September 2016 | Accepted 25 October 2016 | Published 27 October 2016

IRBP deficiency permits precocious ocular development and myopia

Shanu Markand,[1] Natecia L. Baskin,[1] Ranjay Chakraborty,[1,2] Erica Landis,[2,3] Sara A. Wetzstein,[1] Kevin J. Donaldson,[1] Priyanka Priyadarshani,[1] Shannon E. Alderson,[1] Curran S. Sidhu,[1] Jeffrey H. Boatright,[1,2] P. Michael Iuvone,[1,4] Machelle T. Pardue,[1,2,3,5] John M. Nickerson[1]

[1]Department of Ophthalmology, Emory University, Atlanta, GA; [2]Atlanta Veterans Administration Center of Visual and Neurocognitive Rehabilitation, Decatur, GA; [3]Neuroscience Program, Laney Graduate School, Emory University, Atlanta, GA; [4]Department of Pharmacology, Emory University, Atlanta, GA; [5]Department of Biomedical Engineering, Georgia Institute of Technology and Emory University, Atlanta, GA

Purpose: Interphotoreceptor retinoid-binding protein (IRBP) is abundant in the subretinal space and binds retinoids and lipophilic molecules. The expression of IRBP begins precociously early in mouse eye development. IRBP-deficient (KO) mice show less cell death in the inner retinal layers of the retina before eyelid opening compared to wild-type C57BL/6J (WT) controls and eventually develop profound myopia. Thus, IRBP may play a role in eye development before visually-driven phenomena. We report comparative observations during the course of the natural development of eyes in WT and congenic IRBP KO mice that suggest IRBP is necessary at the early stages of mouse eye development for correct function and development to exist in later stages.

Methods: We observed the natural development of congenic WT and IRBP KO mice, monitoring several markers of eye size and development, including haze and clarity of optical components in the eye, eye size, axial length, immunohistological markers of differentiation and eye development, visually guided behavior, and levels of a putative eye growth stop signal, dopamine. We conducted these measurements at several ages. Slit-lamp examinations were conducted at post-natal day (P)21. Fundus and spectral domain optical coherence tomography (SD-OCT) images were compared at P15, P30, P45, and P80. Enucleated eyes from P5 to P10 were measured for weight, and ocular dimensions were measured with a noncontact light-emitting diode (LED) micrometer. We counted the cells that expressed tyrosine hydroxylase (TH-positive cells) at P23–P36 using immunohistochemistry on retinal flatmounts. High-performance liquid chromatography (HPLC) was used to analyze the amounts of dopamine (DA) and 3,4-dihydroxyphenylacetic acid (DOPAC) at P7–P60. Monocular form deprivation in the right eye was induced using head-mounted goggles from P28 to P56.

Results: Eye elongation and eye size in the IRBP KO mice began to increase at P7 compared to the WT mice. This difference increased until P12, and the difference was maintained thereafter. SD-OCT images in live mice confirmed previously reported retinal thinning of the outer nuclear layer in the IRBP KO mice compared to the WT mice from P15 to P80. Slit-lamp and fundoscopy examination outcomes did not differ between the WT and KO mice. SD-OCT measurements of the optical axis components showed that the only factor contributing to excess optical axis length was the depth of the vitreous body. No other component of optical axis length (including corneal thickness, anterior chamber depth, and lens thickness) was different from that of the WT mouse. The refractive power of the IRBP KO mice did not change in response to form deprivation. The number of retinal TH-positive cells was 28% greater in the IRBP KO retinas compared to the WT mice at P30. No significant differences were observed in the steady-state retinal DA or DOPAC levels or in the DOPAC/DA ratios between the WT and IRBP KO mice.

Conclusions: The IRBP KO mouse eye underwent precocious development and rapid eye size growth temporally about a day sooner than the WT mouse eye. Eye size began to differ between the WT and KO mice before eyelid opening, indicating no requirement for focus-dependent vision, and suggesting a developmental abnormality in the IRBP KO mouse eye that precedes form vision–dependent emmetropization. Additionally, the profoundly myopic KO eye did not respond to form deprivation compared to the non-deprived contralateral eye. Too much growth occurred in some parts of the eye, possibly upsetting a balance among size, differentiation, and focus-dependent growth suppression. Thus, the loss of IRBP may simply cause growth that is too rapid, possibly due to a lack of sequestration or buffering of morphogens that normally would bind to IRBP but are unbound in the IRBP KO eye. Despite the development of profound myopia, the DA levels in the IRBP KO mice were not statistically different from those in the WT mice, even with the excess of TH-positive cells in the IRBP KO mice compared to the WT mice. Overall, these data suggest that abnormal eye elongation in the IRBP KO mouse is independent of, precedes, and is epistatic to the process(es) of visually-driven refractive development.

Correspondence to: John M. Nickerson, Department of Ophthalmology, Emory University, B5602, 1365B Clifton Road, NE, Atlanta, GA 30322; Phone: (404) 778 4411; FAX: (404) 778 2231; email: litjn@emory.edu.

Interphotoreceptor retinoid-binding protein (IRBP; gene symbol, *RBP3;* Gene ID 19661; OMIM 180290) is found in high abundance and is the major soluble protein of the subretinal space, also known as the interphotoreceptor space [1]. IRBP binds several types of retinoids and lipids with high affinity [2-4]. It has been proposed that the chief functions of IRBP are to protect retinoids from damage and to protect adjacent biologic membranes from damage by retinoids [3,5]. Much is now known about the binding sites of IRBP through elegant studies of the three-dimensional (3D) structure of parts of the protein [6]. IRBP also functions in mediating the transfer of retinoids between the RPE and photoreceptor cells, most likely by selectively storing retinoids to govern the rate of dark adaptation [7,8].

Arguments have been marshaled that IRBP plays several roles in the classical visual cycle [9-11]. A second visual cycle [12,13] may be superimposed that is selective for the rapid rates of cone dark adaptation involving IRBP and the transport of retinoids from Müller cells to cone photoreceptors [14,15]. More recently, a possible role for IRBP [16] in adaptive potentiation [17] has been demonstrated.

Mutations in the *RBP3* gene cause retinitis pigmentosa [18], and recently, a causative lesion in the *RBP3* gene was discovered in two new families [19]. The rs11204213 [Val884Met] polymorphism in the *RBP3* gene is associated with differences in corneal curvature and axial length [20]. To discover whether the absence of the IRBP gene (a null mutation) causes eye disease, we and others have investigated a knockout of the IRBP gene in the mouse [21,22]. It is clear that the absence of IRBP results in the rapid but partial loss of photoreceptor cells [22,23] followed by slow but complete loss of the retina with age.

Previously, we detected early changes in eye development in the IRBP knockout (KO) mouse that result in an enlarged, heavier, and profoundly myopic eye [22]. We detected early changes in eye dimensions at P10 but not earlier [22], but we did not explore the mechanism. Here, we refine the onset of myopia and the elongation of specific eye compartments in the living IRBP KO mouse.

The processes and mechanisms of eye growth require continual adjustment during the entire period of development and maturation to match eye size with refractive power as a vertebrate animal grows and reaches maturity [24]. Once the eye opens, the process of emmetropization plays a dominant role in altering eye size to carefully place the plane of focus on the neural retina [25]. The peripheral retina is capable of inducing myopia, and only parts of the retina may be necessary for emmetropization [26-28]. Refractive development has been manipulated experimentally with optics, drugs, genetics, and lighting to understand the mechanisms of form-dependent emmetropization [29]. Growth and growth-stop signals are transmitted from the neural retina locally in the eye by signals that act on the sclera where selective growth on the optical axis may occur. Several signaling mechanisms and small molecules act as messengers. These include but are not limited to dopamine, a growth-stop signal [30,31], and retinoic acid, a growth signal [32,33] which act on different parts of the eye [34-36].

The relationships between growth control mechanisms in early development and after eye opening are unclear. Are many of the same pathways shared? Are they independent? Are they partially networked? To define these growth pathways, mechanisms, and potential interrelationships, we proposed three hypotheses for the roles of IRBP in determining eye size.

1. Due to posterior subcapsular cataracts caused by many different retinal degenerations [37-39], one hypothesis is that in the IRBP KO mouse, the optical media (the cornea, anterior chamber, lens, or vitreous) are turbid or hazy obscuring form vision and causing profound myopia, while in the wild-type (mouse) the media are clearer, resulting in normal refractive growth.

2. Another hypothesis (which we first tested in [22]) is that when IRBP is missing, normal vision-dependent refractive growth is affected.

3. Another hypothesis is that the effect(s) of IRBP on eye growth is (are) independent of, precede, and are epistatic to vision-dependent refractive pathways.

Sharp and clear images of the fundus and spectral domain optical coherence tomography (SD-OCT) through the optical media, and slit-lamp exams would establish that all eyes were transparent and free of particulates that scatter light. This finding would discount the “turbidity myopia” caused by the retinal degeneration hypothesis. To test the remaining hypotheses, we looked for early eye size differences before eye opening, as these early changes would not be vision or form dependent (and thus not part of visually-driven refractive growth) although they might be light dependent and require a functioning vitamin A cycle. We accurately timed the first differences in eye size between the IRBP KO and WT mice to test whether abnormal eye growth in the IRBP KO mouse begins well before eye opening, suggesting that pathways of refractive growth are not part of the early abnormal eye growth of the IRBP KO mouse.

Second, we asked whether there are changes in eye size that correlate with changes in dopamine levels or the number of tyrosine hydroxylase–positive (TH-positive) cell

counts. We expected that decreased dopamine levels would be detected in the abnormal elongation of the IRBP KO mouse eye, if dopamine were a critical signal that stops excessive eye growth (as shown in refractive growth). Similarly, we might expect fewer TH-positive cells in the IRBP KO mice compared to the WT mice if these cells were part of IRBP-dependent suppression of eye growth.

Third, we conducted form deprivation experiments. We hypothesized that if IRBP has an essential role in vision- and focus-dependent emmetropization (as opposed to a focus-independent eye growth mechanism), then goggling with diffusers ought to increase the myopic shift of the IRBP KO mouse except if myopia is at the maximum and the eye cannot become any more myopic despite deprivation.

The results of these experiments, as described below, support a direct role for IRBP in eye growth before visually-driven refractive development. This suggests that the role of IRBP in the determination of eye size is manifested at an earlier regulatory point and is completely independent of the process of vision-dependent refractive growth. It is clear that IRBP contributes greatly to the size of the eye and the processes of eye elongation.

METHODS

Mouse husbandry: Mouse care and handling were approved by the Emory University Institutional Animal Care and Use Committee and adhered to standards recommended by the Association for Research in Vision and Ophthalmology (ARVO) and the Association for Assessment and Accreditation of Laboratory Animal Care (AAALAC). C57BL/6J (WT) and congenic IRBP KO mice were used that had been backcrossed more than ten times to WT. The WT and IRBP KO mice colony is routinely screened for the *Crb1*$^{rd8/rd8}$ (rd8) mutation [40]. The WT and IRBP KO mice used in the current study showed the absence of the rd8 mutation. Mouse housing conditions and diet have been described [41]. The Emory University Division of Animal Resources housed and managed mice. Mice were housed at 23 °C on a 12 h:12 h light-dark Cycle and were given and standard mouse chow (Lab Diet 5001; PMI Nutrition Inc., LLC, Brentwood, MO) and water ad libitum. At 9:00 AM in the morning, we searched for new litters. New pups were defined as P1 if they were detected in the 9:00 AM census. The number of mice used per experiment is given in the Results and in each figure and table legend.

Slit-lamp examination: A slit lamp (Carl Zeiss, SL 130, Dublin, CA) was used to examine the mouse eyes. To test whether the optical media were clear in IRBP KO mice, we subjected the WT (n = 5) and IRBP KO (n = 6) mice at P21 to slit-lamp examinations. An examiner who was masked regarding the genotype of the mouse conducted the assessment. An average grading score (0–4) was given for the cornea and lens with a lower grade representing clear structures [42,43]. A Mann–Whitney test was used to assess the statistical significance between groups.

SD-OCT and fundoscopy: A Micron IV SD-OCT system and a fundus camera were used (Phoenix Research Labs, Pleasanton, CA) to analyze retinal morphology in the WT and IRBP KO mice at P15 (WT, n = 5; KO, n = 10), P30 (WT, n = 8; KO, n = 6), P45 (WT, n = 7; KO, n = 8), and P80 (WT, n = 5; KO, n = 7). Image-guided OCT images were obtained for the left and right eyes after a sharp and clear image of the fundus (with the optic nerve centered) was obtained. SD-OCT was a circular scan about 100 µm from the optic nerve head. Fifty scans were averaged. The retinal layers (indicated on the figure images) were identified according to published nomenclature [44,45]. Total retinal thickness and photoreceptor layer thickness were analyzed.

Keratometry: An automated keratometer was used to measure the corneal radius of curvature in the WT (n = 3) and IRBP KO (n = 5) mice at P53 to P55 [46]. The mean corneal radius of curvature (± SD) was recorded. An unpaired two-tailed Student *t* test with the Welch correction was used to assess statistical significance.

Whole-eye biometry: The WT and IRBP KO mice at P30 (WT, n = 8; KO, n = 6), P45 (WT, n = 7; KO, n = 8), P55 (WT, n = 3; KO, n = 5) and P80 (WT, n = 5; KO, n = 7) were subjected to *in vivo* whole-eye biometrical imaging using a Bioptigen R4310 deep imaging SD-OCT system (Leica Microsystems, Durham, NC). Post-imaging analysis included measurement of the following parameters: central corneal thickness (CCT), anterior chamber depth (ACD), lens thickness (LT), vitreous chamber depth (VCD), retinal thickness (RT), and total ocular axial length. The mean thickness (± standard deviation, SD) was recorded. Two-way ANOVA with a Tukey test was used to assess statistical significance.

Metrics and metrology: Mice were euthanized with CO_2 asphyxiation and cervical dislocation before eye dissection, according to protocols approved by the Emory University IACUC and ARVO guidelines. After the mice were euthanized, each eye was removed with forceps, and the extraocular fat and muscles were removed. The optic nerve was cut to leave no stump. Eye weights were recorded with an A-160 analytical balance (Denver Instruments; Fisher Scientific, Pittsburgh, PA). Eye dimensions on three axes were obtained with a light-emitting diode (LED) noncontact micrometer (LS-7030; Keyence Inc., Schaumburg, IL) as described earlier [47] at P5 (WT, n = 10; KO, n = 9), P6 (WT, n = 8; KO, n =

10), P7 (WT, n = 4; KO, n = 4), P8 (WT, n = 6; KO, n = 6), P9 (WT, n = 6; KO, n = 8), and P10 (WT, n = 5; KO, n = 3).

Histology and immunohistochemistry: Routine paraffin-embedded histology with hematoxylin and eosin (H&E) staining, plastic sectioning, staining with toluidine blue, and morphometric measurements were conducted as previously described [22,48]. We detected TH-positive cells in the inner nuclear layer (INL) by performing immunohistochemistry with primary anti-TH antibodies raised in rabbits (Pel-Freez Biologicals; Little Rock, AR). The secondary antibodies against the primary antibody were donkey anti-rabbit Alexa Fluor 488 from Life Technologies, Inc. (Carlsbad, CA). The ages and numbers of the mice were P23 (WT, n = 6; KO, n = 6), P26 (WT, n = 6; KO, n = 5), P30 (WT, n = 5; KO, n = 7), and P36 (WT, n = 10; KO, n = 13). Briefly, the cornea was perforated with a 27 gauge beveled needle, and the eye was fixed for 10 min at room temperature in freshly prepared 4% paraformaldehyde in Dulbecco's PBS (1X ; 2.66 mM KCL, 1.47 mM, KH_2PO_4,137.93 mM NaCl,8.05 and mM Na_2HPO_4-$7H_2O$,pH 7.4; without calcium or magnesium). An eyecup lacking the lens was dissected with iridectomy scissors. The eyecup was filled with 2 mg/ml hyaluronidase (Type IV-S H3884; Sigma-Aldrich, St. Louis, MO) and incubated for 30 min at 23 °C. The eyecup was frozen at −80 °C and thawed at 23 °C to further permeabilize the retina. The retina was removed from the underlying RPE and was flatmounted on a glass slide with the photoreceptor cells face down inside a silicone gasket [48]. Retinas were blocked in 0.25% (V/V) Triton X-100 in PBS and 2% (V/V) normal donkey serum (NDS) overnight at 4 °C, rinsed three times in PBS for 5 min each and then incubated at 4 °C for 3 days in the rabbit anti-rat TH primary antibody at 1:250 dilution in PBS with 0.25% (V/V) Triton X-100 and 2% NDS. The retinas were washed three times in PBS, 5 min each, and incubated in the secondary antibody at 1:500 dilution in PBS with 0.25% (V/V) Triton X-100 in darkness at 4 °C overnight. Retinas were mounted in Vectashield Hardset (Vector Labs Inc., Burlingame, CA), dried for 1 to 2 days at 4 °C in the dark, and imaged with a Nikon C1 confocal microscope (Nikon Instruments, Melville, NY) as described [49,50]. The focal plane was adjusted to image and count TH-positive cells in the INL (dopaminergic amacrine cell bodies).

DA and DOPAC measurements: For the DA and DOPAC analyses conducted in the neural retina, the eyes were harvested, and the neural retina was dissected from the eye as previously described [51] at P7 (WT, n = 7; KO, n = 10), P10 (WT, n = 9; KO, n = 9), P12 (WT, n = 8; KO, n = 9), P23 (WT, n = 9; KO, n = 8), P26 (WT, n = 10; KO, n = 10); P36 (WT, n = 9; KO, n = 12), and P60 (WT, n = 9; KO, n = 9). The retinas were homogenized in 0.2 N perchloric acid containing 0.01% sodium metabisulfite and centrifuged; the supernatant fractions were analyzed with high-performance liquid chromatography (HPLC; Agilent, Santa Clara, CA) eluted with an isocratic mobile phase (5% (V/V) acetonitrile, 0.32 mM sodium octylsulfate, 50 mM sodium phosphate, 0.1 mM EDTA, pH 2.7 to 3.2) on a 5 µm Ultrasphere 250 × 4.6 mm C18 column (catalog number 235,329; Hichrom, Ltd., Reading, UK) with reverse phase chromatography and an electrochemical detection system [30,52,53].

OPL grading: Paraffin and plastic sections of WT (n = 16) and IRBP KO (n = 8) mouse retinas at P5 and P6 were ranked by three observers who were masked regarding the genotype of the mouse. Grade 1 included a distinct and continuous outer plexiform layer (OPL). Grade 2 represented a less distinctive OPL, and grade 3 had little to no evidence of an OPL. A Mann–Whitney test was used to assess statistical significance between groups.

Goggling: A diffuser lens covering the right eye was connected to a head pedestal to induce visual form deprivation in mice from P28 to P56, as previously described [54]. The diffusers were plano contact lenses made from polymethyl methacrylate (PMMA; X-Cel Contacts, Duluth, GA) painted with partially translucent white paint (Top Speed Fast Dry Nail Enamel, 0,429,920; Revlon, New York, NY). The goggles were counterbalanced to ensure even weight distribution. The contralateral (left) eyes were not goggled. An infrared automated photorefractor [55] was used as previously described [22,54,56]. A two-way repeated-measures ANOVA with the Holm-Sidak test was used to assess statistical significance between the groups.

Visual acuity: Optokinetic tracking responses (OKTs) were obtained with an optomotor system (Cerebral Mechanics Inc., Lethbridge, Canada). Visual acuity was measured at 100% contrast as previously described [57-59]. Three experienced observers evaluated mice from different litters at P26 (KO, n = 6), P30 (WT, n = 8; KO, n = 2), P36 (KO, n = 2), P45 (WT, n = 7; KO, n = 1), P95–P96 (WT, n = 6; KO, n = 7), and P265 (KO, n = 6).

Statistical analysis: Data from each group are summarized as the mean ± standard deviation with the sample size indicated in each figure, legend, and table. In each sample group, mice from different litters were included. Analysis was performed with an unpaired two-tailed Student *t* test with the Welch correction, ANOVA with Tukey's test, or other tests as

indicated in the text or figure legend. GraphPad Prism 6.0 for Mac OS X (GraphPad Software, Inc., La Jolla, CA) was used.

RESULTS

Optical clarity, fundus imaging, keratometry, and SD-OCT: One explanation for the KO effects on axial elongation is that the media were turbid, cloudy, and obscured form, leading to eye elongation by form deprivation myopia as routinely occurs in retinal degenerations that are associated with posterior subcapsular cataracts [37,38]. Thus, an early experiment was to test the clarity of the optical media in the two mouse strains (WT and IRBP KO) at four ages: one (P15) just after eye opening, one after the burst of photoreceptor cell death had occurred in the IRBP KO mice (P30), and two later time points (P45 and P80) in the living mice. About 50% of the IRBP KO mice (n = 10) at P15 had a slightly cloudy optical path. In the WT mice, only one of five mice had a cloudy axis at P15. However, the optical media (the cornea, anterior chamber, lens and vitreous) all were equally clear and transparent in both strains and at all other ages as established by sharp and distinctive layering within the retina of the same mice with noninvasive SD-OCT (Micron IV) and by equally crisp fundus photographs (Figure 1A–H). To test whether the curvature of the cornea is altered in IRBP KO mice, we measured the corneal radius of curvature in the WT and IRBP KO mice at P55. We observed no significant difference between the corneal curvature of the WT mice and that of the IRBP KO mice (mean = 1.413±0.012 mm for the KO mice, n = 8; for WT mice, 1.392±0.015 D, n = 3; p = 0.3301, unpaired two-tailed Student *t* test with the Welch correction).

We next examined the eye with a slit lamp to evaluate the clarity in the cornea and lens. We did not detect any obvious opacity or haze at P21 in either eye in five KO mice and five WT mice. The slit-lamp exam revealed no significant difference in the average grading score for the IRBP KO and WT mice (the Mann–Whitney test, cornea, p = 0.318 and lens, p = 0.0541). These results did not support the hypothesis that cloudiness, corneal defects, lens defects, or back scattering of light prevented form detection in the IRBP KO mouse eye, which alone would have explained profound myopia in the IRBP KO mouse.

SD-OCT images from individual living mice verified previous histological work [22] on enucleated eyes that identified substantial outer nuclear layer (ONL) layer loss after P15 and before P30, P45, and P80 (Figure 1; statistics given in Table 1, all p<0.0001) in the IRBP KO mouse eye. At P15, the ONL was 13% less thick in the IRBP KO mouse eye than in the WT mouse eye. At P30, 34.4% of the ONL thickness was lost in the IRBP KO mouse eye compared to the WT mouse eye at the same age. At P45–P80, similar thinning in ONL thickness was observed in the IRBP KO mouse eye compared to the WT mouse eye (35.9% at P45), and 38.6% loss of the ONL in the IRBP KO mouse eye at P80 compared to the WT mouse eye. Total retinal thickness was lost in the IRBP KO mouse eye relative to the WT mouse eye following the same pattern (Table 1) with almost all of the differences between the KO and WT mouse eyes accounted for by the profound loss of ONL thickness. A noteworthy observation was an 11% increase in photoreceptor thickness in the WT mouse eye from P15 to P30 (88.1±1.42 to 97.8±3.53 µm, respectively, which was statistically significant at p<0.01; Tukey's test). This thickness increase agrees with our previous observation [22] of a similar increase in photoreceptor nuclei counts across the ONL between P15 and P30 in histological cross sections.

Fundus imaging (Figure 1) detected no mottling at P15 in either the IRBP KO or WT mice. However, from P30 to P80, there was readily observed mottling at the layer of the outer segments and the RPE in the IRBP KO mice, but no such mottling was observed in the WT mice at P30–P80. These images highlight the subtle character of the changes in the eye caused by the absence of IRBP until after P15 and the profound ONL loss in a tight time window from P23 to P30 as previously observed in histological sections [22]. Mottling of the IRBP KO fundus coincided temporally with ONL loss; however, any causal relationship of mottling and ONL loss is not understood.

Table 2 illustrates axial measurements shown with SD-OCT (Bioptigen, model 4310) from living mice. We obtained the total optic axis length (anterior cornea to the RPE, an internal diameter measure), CCT, ACD, lens thickness, vitreous depth, and retina thickness. The total of these measurements summed to about 50 µm thinner than the measurement from the LED noncontact micrometer for external eye size [47]. This difference in thickness was contributed by the choroid and the sclera. The chorioscleral thickness, estimated from the difference, was the same as the measurement of the chorioscleral thickness from histological sections. These measurements were all consistent internally and with previous histological and LED micrometer measurements [22], which validated the SD-OCT measurements in live mice.

The vitreous chamber was substantially deeper (about 60% more) in the IRBP KO mice than in the WT mice at all four ages (P30, P45, P55, and P80; Table 2). This difference accounted for all the excessive eye elongation in the IRBP KO mouse over the WT mouse. None of the other biometric parameters were significantly different in the IRBP KO

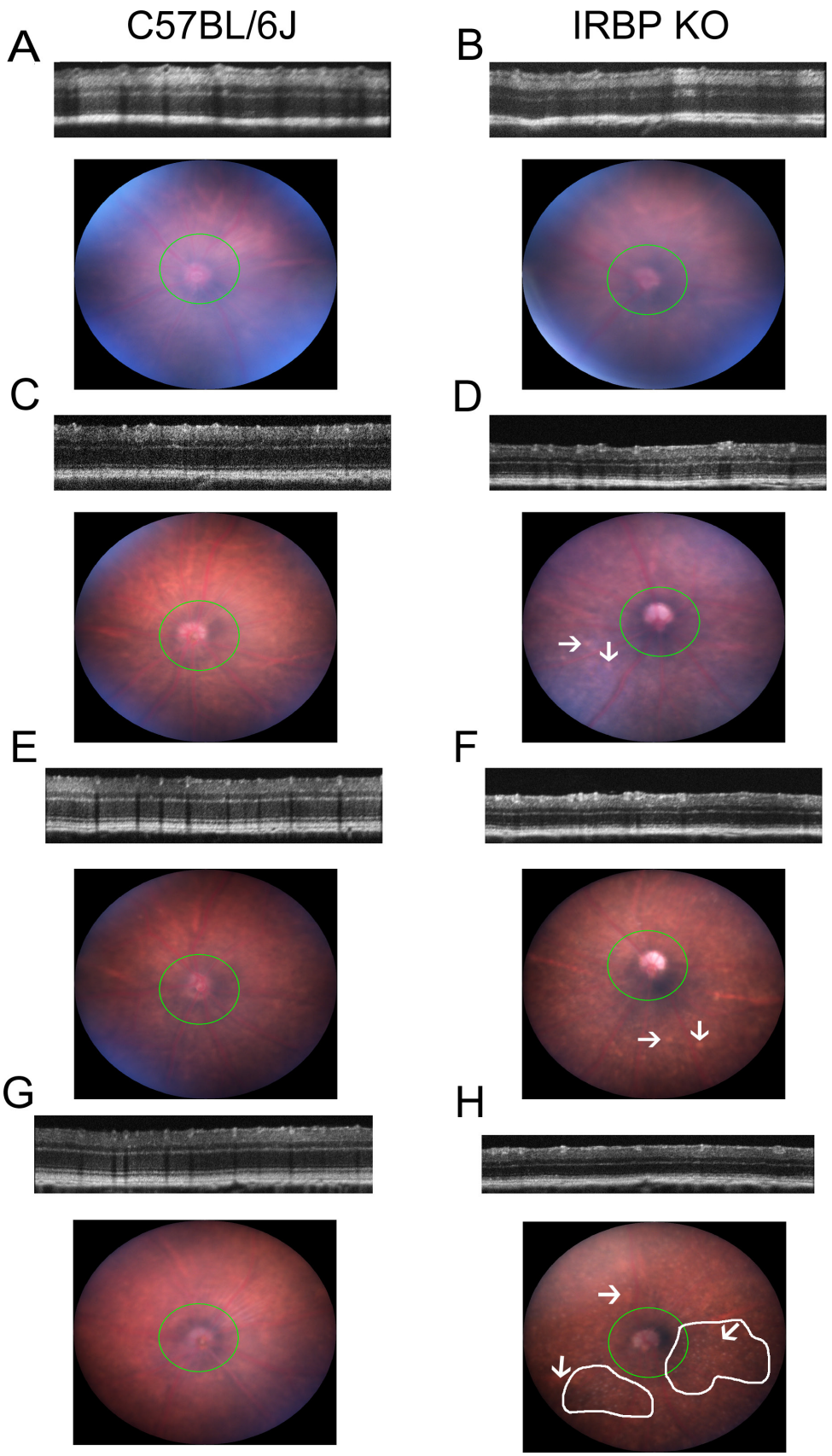

Figure 1. Fundus photos and SD-OCT images of the IRBP KO and WT mouse eye. Spectral domain optical coherence tomography (SD-OCT) and fundus images were obtained non-invasively in living mice at different ages (P15, P30, P45, and P80) in this representative figure. **A**–**H** illustrate clear optical media in the wild-type (WT) and interphotoreceptor retinoid-binding protein (IRBP) knockout (KO) mouse eye. No cloudiness or haze was detected in the cornea, anterior chamber, lens, or vitreous at P30 (**C**–**D**), P45 (**E**–**F**), and P80 (**G**–**H**) in the IRBP KO or WT mouse. Slight haze or cloudiness was observed at slightly greater levels in the P15 KO mouse fundus (**B**) than in the WT mouse fundus (**A**), but the SD-OCT images were equally crisp. This cloudiness appeared to be caused by the presence of residual hyaloid vasculature near the optic nerve detected in histological sections. In the IRBP KO mouse, outer nuclear layer (ONL) thickness is lost between P15 and P30 in the living KO mouse eye. The fundus photos showed mottling at P30, P45, and P80 that was not detected at P15 in the same IRBP knockout mouse (indicated by arrows). No mottling was observed in the WT mice at any age. At P80, distinct focal white spots were observed in the IRBP KO mice (marked by a white boundary). There was a loss in thickness in the ONL of the P15–P80 KO mouse compared to the P15–P80 WT mouse. These live images validate previous work on histological sections from enucleated eyes [22]. The SD-OCT images established that the retinal and ONL thickness develops fully, and then cells are lost through a degenerative process by P30.

Table 1. Thinning of the ONL and retina of the IRBP KO relative to the WT.

Age	Total Retina Thickness Mean ± standard deviation		Two-way ANOVA with Tukey's test	Photoreceptor Thickness Mean ± standard deviation		Two-way ANOVA with Tukey's test
	WT (n=5)	KO (n=10)		WT (n=5)	KO (n=10)	
P15-P17	227.88±3.87	200.92±10.21	****	88.10±1.42	76.72±3.75	****
	WT (n=5)	KO (n=8)		WT (n=5)	KO (n=8)	
P30	220.19±3.63	166.30±3.89	****	97.81±3.53	64.14±2.33	****
	WT (n=6)	KO (n=8)		WT (n=6)	KO (n=8)	
P45	218.61±5.65	166.59.88±3.55	****	99.24±4.82	63.62±1.47	****
	WT (n=5)	KO (n=7)		WT (n=5)	KO (n=7)	
P80-P81	215.09±2.72	163.97±3.26	****	101.95±4.00	62.63±1.68	****

Total retinal thicknesses and photoreceptor cell layer (ONL+IS+OS) thicknesses were measured with a Micron IV SD-OCT in WT and KO mice (P15-P80). The present measurements were taken in a ring around the optic nerve head at about 100 microns radially, indicating a loss throughout regardless of vertical or horizontal orientation. Values are reported in microns. Comparisons were made by ANOVA and Tukey test. **** Represents $p<0.0001$.

and WT mice. The lens of the IRBP KO mouse eye was the same thickness as in the WT mouse eye at equivalent ages. These lens thickness measurements with SD-OCT in live mice are the same as those we previously reported with an LED micrometer in unfixed harvested tissue [22] and with measurements of histological H&E-stained sections of the lens after formalin fixation or freeze-substitution and paraffin embedding (data not shown).

Onset of aberrant eye elongation in IRBP KO mice: We previously found changes in the size and axial length in IRBP KO mice as early as P10 [22]. To refine the onset of KO eye elongation, we studied IRBP KO and WT eyes at 1-day increments from P5 to P10 (Figure 2 and Figure 3). It was clear that the eye weight of the IRBP KO mice began to deviate by P7 (Figure 2), but not at earlier ages, P5 or P6. By P8 and older, the IRBP KO mice had heavier eyes than the WT mice (Figure 2), according to two-way ANOVA with the Sidak multiple comparisons test ($p = 0.0021$). As shown in Figure 3, the IRBP KO animals also showed a trend for longer axial length from P8 onward using the LED non-contact micrometer that became statistically significant at P10 (Appendix 1, panels 3B and 3C). We found that the IRBP KO and WT mouse eyelids opened at the same time (mean = 13.0±0.93 days for the KO mice, n = 8 litters; for the WT mice, 13.8±0.67 days, n = 9 litters; $p = 0.0717$, unpaired two-tailed Student *t* test with the Welch correction). Thus, in the IRBP KO animals, the eyes were heavier and generally longer on the optical axis 6 days before the eyelids opened than in the WT animals.

Morphology of eyes in IRBP KO and WT mice: We did not detect any major histological changes in the structure of the eye, including the retina, lens, cornea, iris, ciliary body, and optic nerve head, with the exception of a small constant thinning of the retinal layers, which began at P7. This thinning was in proportion to the expansion of the eye surface area over which the retina was stretched in a comparison of the IRBP KO and WT mice. These thicknesses are illustrated in Figure 4A (the retina) and Figure 4B–E in Appendix 2.

Developmental maturation in the IRBP KO and WT mice appeared to be similar with the exception of the appearance of the OPL at P5 in the IRBP KO mice. The OPL appeared more distinct, better formed, and more mature in the IRBP KO mice than in the WT mice at P5 (Figure 5; Table 3). However, a day later, the OPL appeared equally mature in the IRBP KO and WT mice, and the same morphologically as assessed with toluidine blue staining of the plastic sections and H&E staining of the paraffin sections (data not shown). Retinal sections from P5 WT (n = 16) and IRBP KO (n = 8) mice were ranked by three blinded observers. Grade 1 was for a distinct, regular, uniform, and continuous OPL. Grade 2 was for a less distinctive, slightly undulating, and interrupted OPL, and grade 3 was for little to no evidence of an OPL. Table 3 shows the scoring of the differences in grading between the WT and IRBP KO mice, and a significant difference between the two strains according to the Mann–Whitney U-test ($p = 0.041$). Subtle changes in specific cell types that required immunostaining are discussed in the following sections.

DA and DOPAC measurements: We measured the DA and DOPAC levels with HPLC. Contrary to expectations, neither DA nor DOPAC decreased in the IRBP KO mice compared to the WT mice (Appendix 3, Figure 6A,B). The ratio of DOPAC to DA remained unaltered (Appendix 3, Figure 6C).

More TH-positive amacrine cells in IRBP KO mouse retinas compared to the WT controls: We examined TH-positive cells in retinal flatmounts to obtain a much larger sampling

Table 2. Excessive axial length in the KO originates solely from an increased vitreous chamber depth.

Dimension	Mean	SD	Sample number	Mean	SD	Sample number	ANOVA p-value Tukey	Significant at p<0.05?
	Wild type P30			**Knockout P30**				
CCT	100.1	10.58	8	109.4	9.18	6	ns	No
ACD	289.6	12.49	8	259.4	14.14	6	ns	No
Lens	1800.9	41.2	8	1787	29.19	6	ns	No
Vitreous	638.4	37.59	8	1018.4	51.26	6	< 0.0001	Yes
Retina	210.5	24.94	8	172	16.39	6	< 0.05	Yes
Total axial length	3067.6	56.52	8	3353.9	35.44	6	< 0.0001	Yes
	Wild type P45			**Knockout P45**				
CCT	87.9	12.13	7	90.27	9.07	8	ns	No
ACD	318.1	15.13	7	296.04	15.99	8	ns	No
Lens	1918.6	38	7	1920.62	30.86	8	ns	No
Vitreous	653.7	15.77	7	971.27	52.03	8	< 0.0001	Yes
Retina	208.9	15.77	7	183.37	15.48	8	ns	No
Total axial length	3224	55.22	7	3475.17	27.58	8	< 0.0001	Yes
	Wild type P53-55			**Knockout P53-55**				
CCT	111	4.4	3	112.6	5.397	5	ns	No
ACD	314.5	4.49	3	294.7	10.92	5	ns	No
Lens	1866	14.93	3	1849	16.74	5	ns	No
Vitreous	564	8.73	3	899.6	15.12	5	< 0.0001	Yes
Retina	274.1	12.7	3	239.4	27.7	5	ns	No
Total axial length	3130	9.91	3	3396	36.34	5	< 0.0001	Yes
	Wild type P80-82			**Knockout P80-82**				
CCT	87.3	7.44	5	95.5	7.61	7	ns	No
ACD	365.2	26.35	5	354.7	33.19	7	ns	No
Lens	2099	81.37	5	2075.5	32.13	7	ns	No
Vitreous	530.3	60.93	5	883.8	18.17	7	< 0.0001	Yes
Retina	222	13.84	5	175	19.59	7	< 0.05	Yes
Total axial length	3359.9	34.21	5	3615	63.63	7	< 0.0001	Yes

Axial measurements were made with a Bioptigen 4310. Axial measurements were collected in the KO versus WT mouse eyes at P30, P45, P54, and P80. All measurements are in microns. ANOVA and a Tukey test were conducted. The essential point of these axial measurements is that the vitreous chamber of the KO was much deeper than the WT, and this accounted for all the excess axial length of the KO mouse. Abbreviations: CCT, central corneal thickness; ACD, anterior chamber depth; Lens, lens thickness; Vitreous, Vitreous Chamber depth; Retina, retina thickness; Length, total axial length from anterior surface of the cornea to the basal face of the RPE.

of TH-positive cells than in standard cross sections. In these flatmounts, we detected about 28% more TH-positive cells in the P30 IRBP KO mice than in the WT mice (Figure 7). These results correlated temporally with our previous studies in which IRBP KO mice did not exhibit any ONL degeneration until P23 and older [22].

Lack of form deprivation myopia in IRBP KO mice: Form deprivation in WT mice results in a myopic shift in refraction [60-62]. In contrast, form deprivation in the IRBP KO

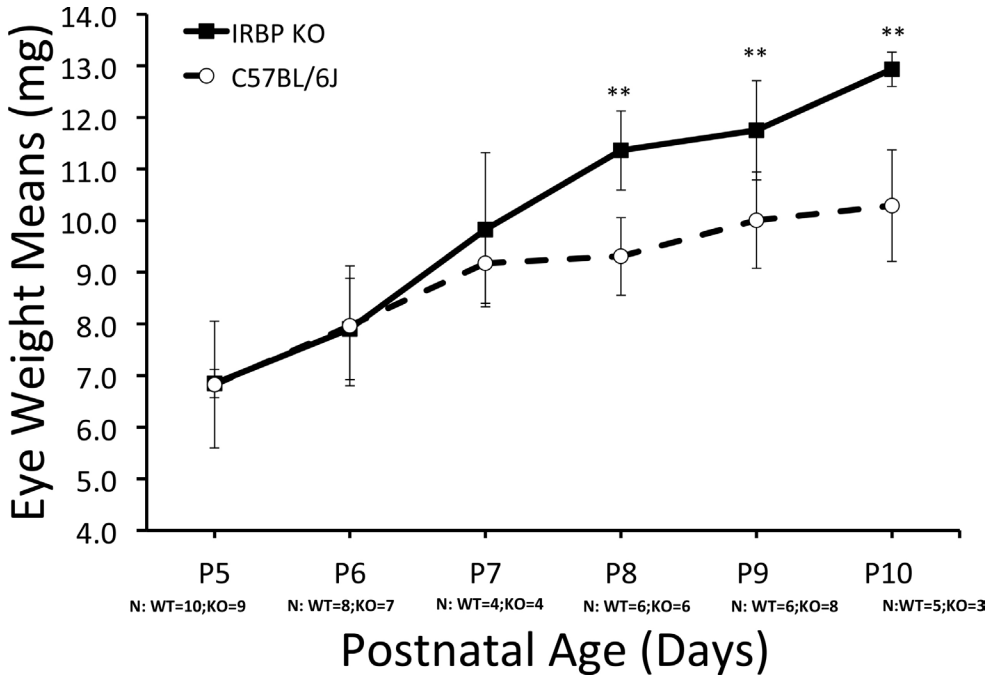

Figure 2. Initiation of abnormal eye size in the IRBP KO mouse. To refine the point in time when the knockout (KO) eye begins to become larger and heavier than the wild-type (WT) mouse eye, we weighed mouse eyes daily from P5 to P10. Eye weight in the interphotoreceptor retinoid-binding protein (IRBP) KO mouse started to increase compared to the WT mouse at P7 (well before eye opening at P13–P14). This difference was significant at P8 and older (** represents $p<0.01$). Eye weights at earlier ages (P5 and P6) were the same in the WT and KO eyes. Sample numbers represent independent mice. Sample numbers at each age and strain are given on the figure. Error bars represent standard deviation.

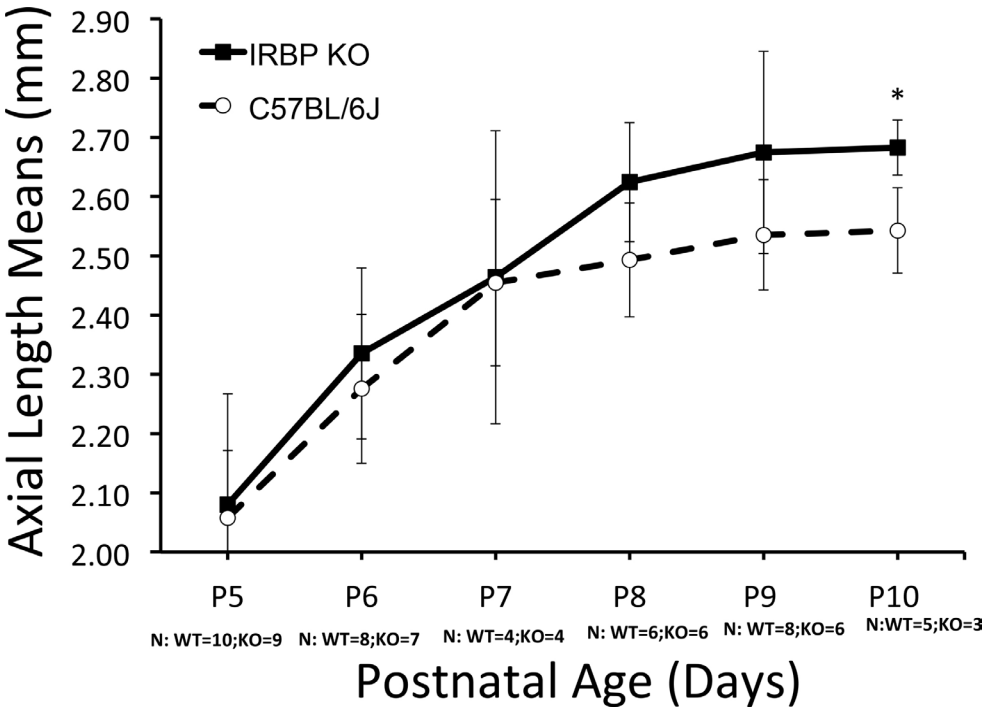

Figure 3. Axial length compared between IRBP KO and WT mice. From P5 to P10, we compared axial length. Axial length was measured with an LED micrometer. At P5–P7, the axial lengths were the same. From P8 and older, the axial length of the knockout (KO) mouse trended longer than that of the wild-type (WT) mouse by about 100 µm. By P10, the lengths were significantly different ($p<0.05$, two-way ANOVA and Tukey test). Sample numbers and groups are the same as in Figure 2. Error bars represent standard deviation. Nasotemporal and superior-inferior measurements are given in Figure 3B,C in Appendix 1.

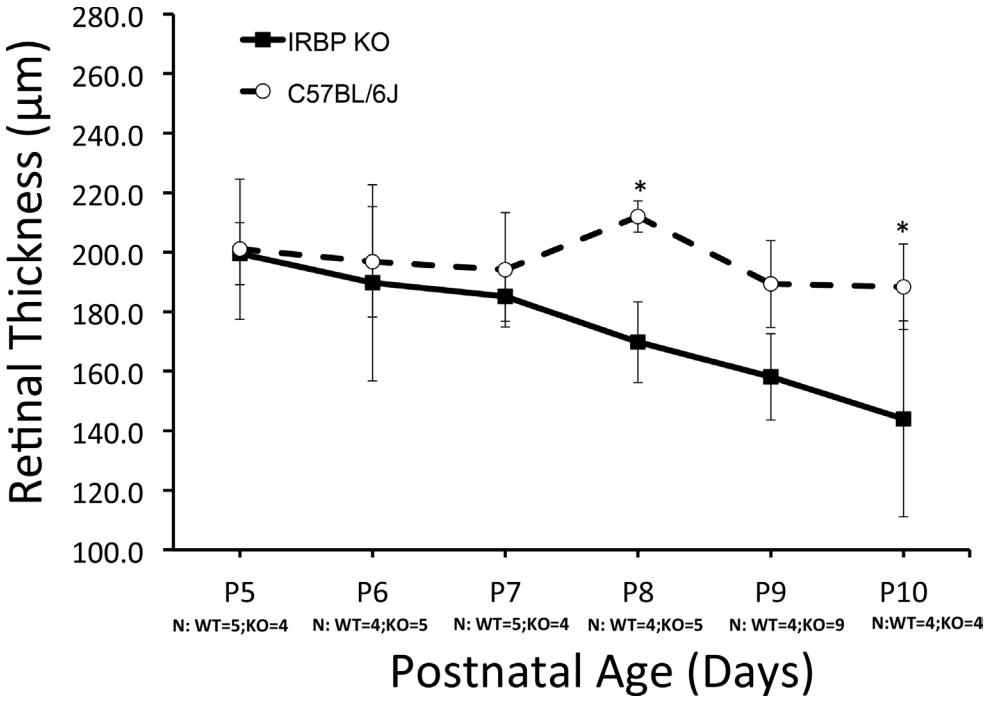

Figure 4. Similarity in scleral and total retinal thicknesses in KO and WT mice. **A**: The indicated layer thicknesses were measured with Longboard software on plastic sections stained with toluidine blue. Thicknesses are expressed in microns. The retinal thicknesses of the knockout (KO) and wild-type (WT) retinas were thinner in the IRBP KO mice than in the WT mice from P7 and later. Sample numbers at each age and strain are given on the figure. Appendix 2, panel **B**: The scleral thickness remained the same. Other individual layer thicknesses were the same. **C**: Choroid thickness. **D**: Inner nuclear layer (INL) thickness. * $p<0.05$; ** $p<0.01$.

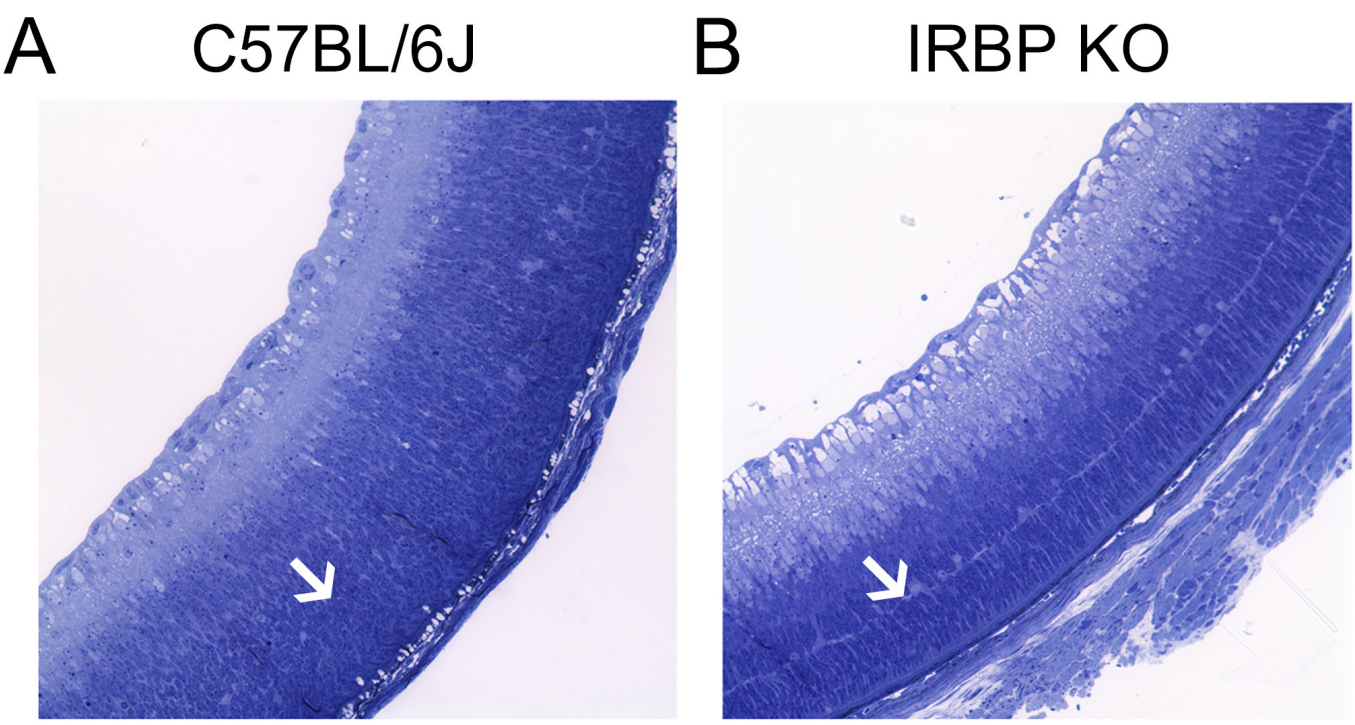

Figure 5. Comparison of retina development between the IRBP KO and WT mice at P5. At P5, the transition from a ventricular zone into the distinctive outer nuclear layer (OPL), outer plexiform layer (OPL), and inner nuclear layer (INL) has taken place in the knockout (KO) mice but lagged in the wild-type (WT) mouse. The OPL (indicated by an arrow) is more distinct and continuous in the interphotoreceptor retinoid-binding protein (IRBP) KO mouse (**B**) than in the WT mouse (**A**) at P5. The potential implications of a better established OPL are lacking IRBP, the retina develops faster, and IRBP normally slows photoreceptors from connecting to horizontal cells and bipolar cells.

Table 3. Evaluation of OPL at P5. A consistent and the earliest detected morphological difference between WT and KO eyes was found in the OPL.

Average grade of the OPL at P5	
WT	**KO**
2.3	1.3
2.7	2.7
3.0	1.0
3.0	1.3
2.3	2.3
2.0	1.3
2.0	2.0
2.0	3.0
2.7	
3.0	
2.7	
3.0	
2.0	
3.0	
2.7	
2.0	
Mean ± SD	
2.53±0.426	1.86±0.746

The OPL appeared to be more clearly recognizable and continuous in the IRBP KO, while the OPL was less distinctive and less continuous in the WT at P5. Histological cross sections of plastic embedded eyes were cut at about one micron in thickness and stained with toluidine blue. Average OPL grades were collected by three blinded independent observers from independent WT and KO mice at P5. A grading scale from 1 to 3 was used. A score of one corresponds to a fully developed and continuous OPL, while a grade of 3 represents little evidence of any detectable OPL. A grade of 2 represents a partially formed and discontinuous OPL. Each row represents one mouse. A significant difference between the two groups was detected by Mann–Whitney U-test (p=0.041).

mice for 4 weeks (from P28 to P56) produced no myopic shift, and the refractive error in the goggled eyes was not significantly different from that in the ungoggled fellow eyes or naïve controls (Figure 8). During the 4 weeks of goggling in the IRBP KO mice, the refractive errors shifted toward more myopia in the goggled eyes, the unmanipulated contralateral eyes, and the eyes of the naïve IRBP KO animals. This age-dependent myopic shift is the same value (about 4 D) as previously observed with ungoggled IRBP KO mice at P30 to P60 [22].

Visual acuity thresholds: The visual acuity of the IRBP KO and WT mice was measured with OKT and compared at several ages (P26–P265). There were no differences in visual acuity between the strains at any of the indicated ages. The responses of the WT mice at all ages were close to 0.383±0.024 c/d. The IRBP KO mice had similar visual acuity (0.386±0.001 c/d) at P26, with a gradual taper to about 0.347±0.002 c/d at P265, representing a slight loss. The overall visual behavior at P265 was unaffected by the reduced thickness of the ONL by about 50%, and by a significant myopic refractive error of about 15 D at the same age. This indicated great resilience of reflexive visual behavior despite these two substantial abnormalities.

DISCUSSION

In mammals, IRBP is abundant in the interphotoreceptor space and binds retinoids, including retinoic acid at high affinity [4]. IRBP is found uniquely in the eye with small amounts of IRBP and IRBP mRNA found in the pineal gland [63,64]. IRBP expression begins precociously early in mouse eye development [65,66]. In the IRBP knockout mouse, a null mutation results in the complete loss of IRBP mRNA and protein, and causes eye size defects and disproportionate eye elongation, leading to profound myopia [22]. There are no known defects in other parts of the body of this KO mouse. For example, the bodyweight of the IRBP KO mouse is the same as that of the WT mouse [22]. In this study, we tested three hypotheses about how IRBP deficiency might cause abnormal eye growth and profound myopia.

First, we proposed that in the IRBP KO mouse, the optical media (the cornea, anterior chamber, lens, or vitreous) are turbid or hazy due to retinal degeneration [37-39]. This would obscure form and cause profound myopia, while in the WT mouse, the media are clear, resulting in normal refractive growth. However, our data indicated that the optical media were equally clear in the living IRBP KO and WT mice, as established by sharp fundus photos, by crisp, detailed layering in the retina with SD-OCT imaging at young ages after eyelid opening, and by nearly identical slit-lamp examinations. These findings disprove the hypothesis that significant turbidity in the optical path of the IRBP KO mouse (blocking form vision) causes excessive eye elongation and profound myopia in the KO mouse.

The only physical factor contributing to excess optical axis length was the depth of the vitreous body (Table 2). No other component of optic axis length (including corneal thickness, corneal curvature anterior chamber depth, and lens thickness) was larger than in the WT mouse. The vitreous is known to be the primary biometric component of axial myopia in several animal models [67,68]. Our finding might suggest that excessive mechanical stretching or elongation

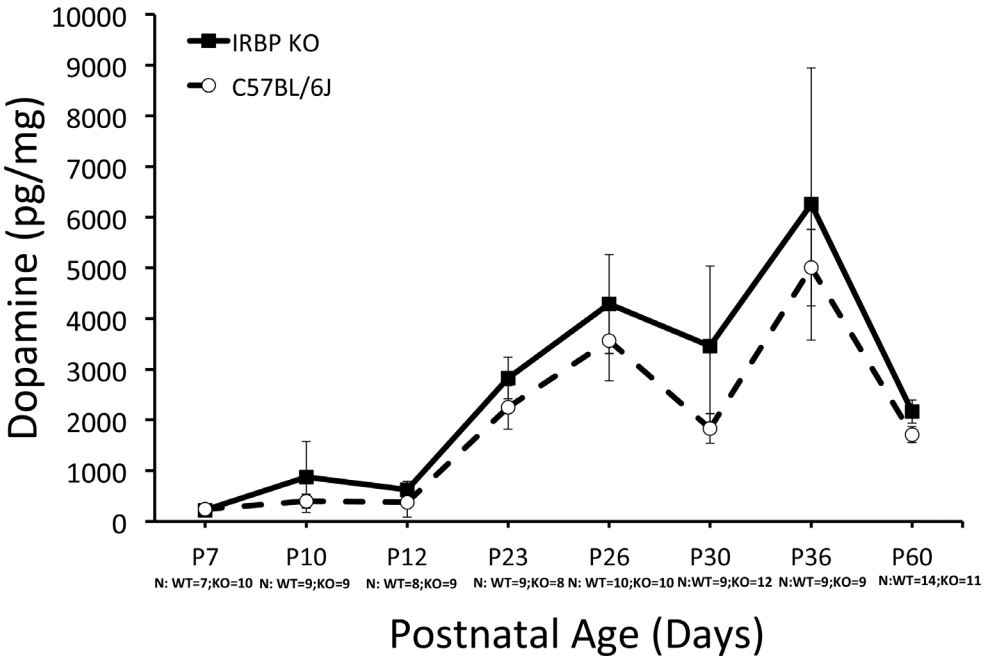

Figure 6. Normal dopamine and DOPAC levels in the IRBP KO mouse compared to the WT mouse. **A**: Dopamine (DA) levels per eye. Appendix 3, panel **B**: 3,4-dihydroxyphenylacetic acid (DOPAC) levels. **C**: DOPAC to DA ratios, respectively. At all time points, DA and DOPAC are the same in the knockout mice (KO) mouse retina as in the wild-type (WT) mouse retina. The ratio of DOPAC to DA remained constant regardless of age or strain.

of the globe is the result of a larger vitreous chamber in the IRBP KO mice or vice versa. Currently, we cannot yet resolve which causes the other. However, it is clear that the only change is in the vitreous chamber depth of the myopic IRBP KO mouse.

Our second hypothesis of altered refraction in the IRBP KO mouse was supported by observation of noticeably heavier and longer eyes in the IRBP KO mice than in the WT mice, with the trend initiating at P7. The early age (P7) when eye size began to differ between the WT and IRBP KO mice occurs 6 days before eyelid opening for both strains (at P13). As the eyelid serves as a diffuser and a filter, the lack of IRBP exerts an effect without relying on focus- or form-dependent vision. In addition, the refractive power in the IRBP KO mice in response to form deprivation was unchanged.

Data from other experiments supported the third hypothesis that the effect(s) of IRBP on eye growth is (are) independent of, precede(s), and is (are) epistatic to the emmetropization pathways. Despite the development of profound myopia, the IRBP KO mouse retinas had the same levels of DA and DOPAC compared to the WT mouse retinas. According to the second hypothesis, we had expected the opposite, that low levels of DA would be associated with accelerated eye growth. We found a small excess of TH-positive cells in the IRBP KO mouse retina compared to the WT mouse retina. These excess TH-positive cells may result from reduced pruning of retinal TH-positive cells in the development of the IRBP KO inner retina. Exposure of the IRBP KO mice to form deprivation goggles did not affect the profoundly myopic KO eye compared to the ungoggled contralateral eye, suggesting that abnormal eye elongation in the IRBP KO mouse is independent of, and precedes the process of emmetropization.

The IRBP KO mouse may exhibit a ceiling effect in that the eye has already reached the maximum size and the maximum axial elongation for a given age. (This may suggest additional mechanisms independent of focus- and form-based emmetropization, as the eye and the mouse body never stop increasing in size and weight according to our previous study [47].) The IRBP KO eye appears incapable of becoming more myopic. Thus, form vision–dependent emmetropization is subordinate to previous eye growth mediated by IRBP. It could be that hyperopic lenses instead of diffusers may be informative.

Despite a large error in refractive power (a 15 D shift toward myopia in the IRBP KO mouse eye versus the WT mouse eye), the optokinetic response pathways were remarkably robust in vivo according to the behavioral reflex measurement as the IRBP KO mice retained the same visual acuity as the WT mice. This may be due to the large depth of focus of the mouse eye [68] or partial regulation of OKT by higher visual centers [69].

A final point is that there was an increase in the thickness of the WT photoreceptor layer in the WT mouse between P15 and P30. This finding matches histological evidence of an increase in nuclear counts and ONL thickness in the mouse

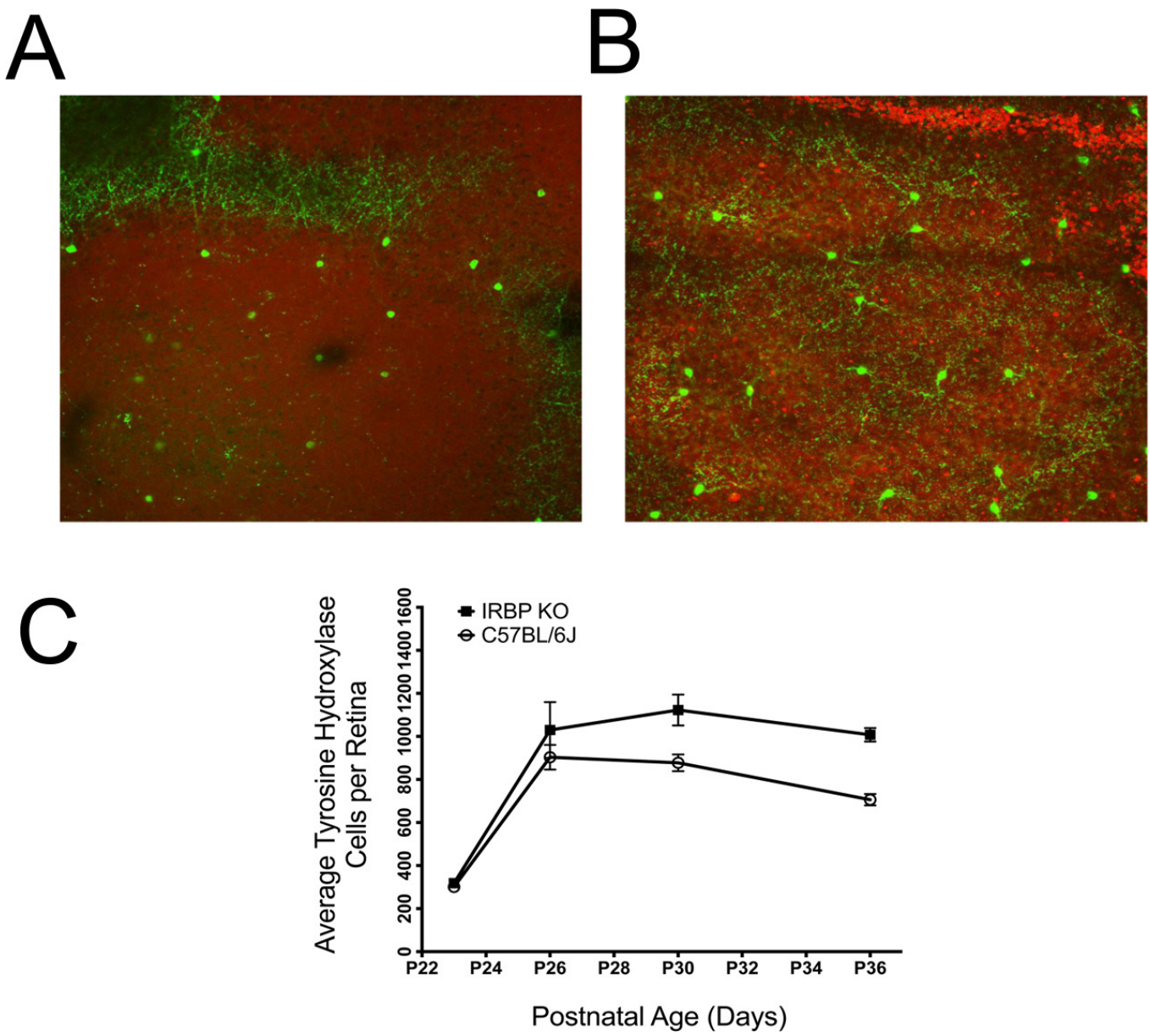

Figure 7. Increased counts of TH-positive cells in the IRBP KO mice compared to the WT mice. Flatmounting of the retina and immunostaining for tyrosine hydroxylase (TH) was conducted on P30 wild-type (WT) mouse eyes (**A**) and knockout (KO) mouse eyes (**B**). Substantially more TH-positive cells were evident in the interphotoreceptor retinoid-binding protein (IRBP) KO retina than in the WT retina. **C**: There was about a 25% increase in the number of TH-positive cells in the inner nuclear layer (INL) of the IRBP KO mouse retina compared to the WT mouse retina at P30. The pattern of excessive TH-positive cells was not evident until P26 and later. This inverse relationship coincides closely with the pattern of a rapid burst of cell death in the ONL of the IRBP KO mouse.

eye peaking at about P30 [22]. The increase in the number of nuclei and the photoreceptor layer thickness implies that an accumulation of photoreceptor cells, swelling of each cell body, or an unrecognized cell type is amassing in the ONL between P15 and P30. Although this is speculative, this could be interesting or important if new cell division in photoreceptors could be encouraged in a retina that is usually thought of as incapable of cell division. This could be a hint about the factor that caused more photoreceptor cells to be laid down between P15 and P30 in the WT mice.

Future experiments beyond the intended scope of this article: We aim to formally test for genetic epistasis. Does the *Rbp3* gene act upstream from putative downstream genes known to

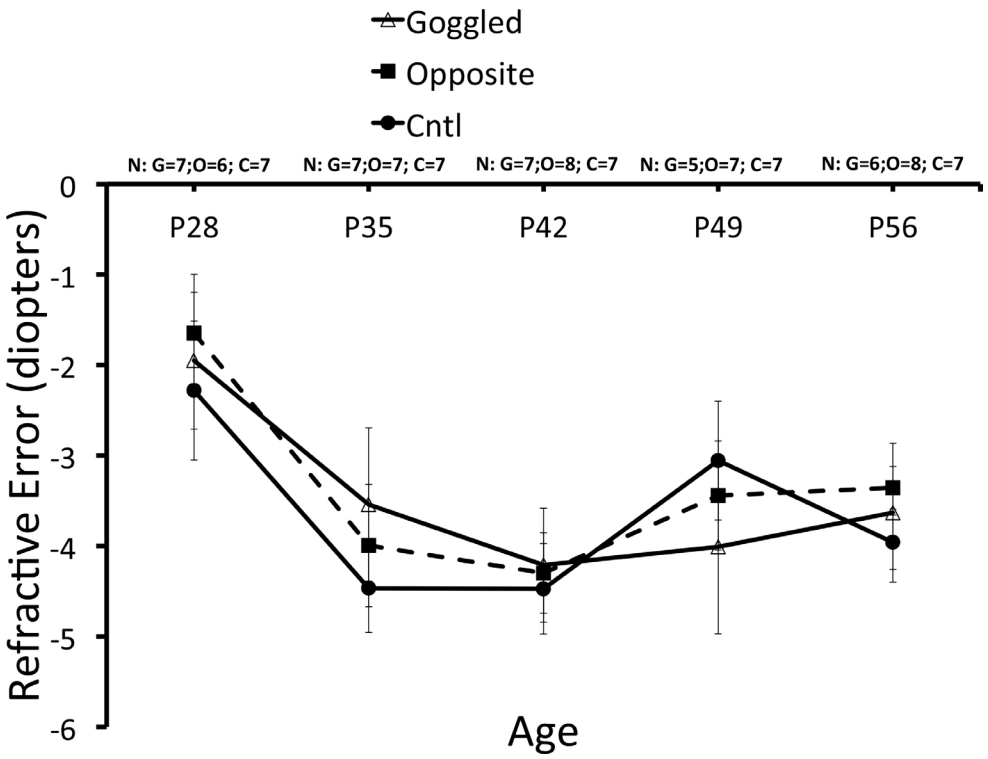

Figure 8. Refractive error of form-deprived right eyes and ungoggled left eyes from IRBP KO mice over time compared to eyes from naïve control mice. In all cases, the refractions remained the same at approximately −4 D (no significant differences on the Holm-Sidak test, $p>0.05$) regardless of age or the length of goggling. This suggests a ceiling effect, and that the role of the interphotoreceptor retinoid-binding protein (IRBP) is manifested in processes that precede focus- or form-dependent vision adjustments toward refractive growth.

be part of visually-driven refractive development, including potential candidates such as *Egr-1* [70]?

Experiments with agonists and antagonists of morphogens may help to test whether vision-dependent mechanisms and the earlier non-image forming development of eye size rely on the same or different pathways to adjust eye size as neonatal mice mature to adulthood. This could include the interference or delivery of excess potential IRBP substrates to determine their role in morphogenesis.

Form vision–dependent emmetropization is subordinate to previous eye growth mediated by IRBP according to our goggling experiment, which employed diffusers. It could be that hyperopic lenses instead of diffusers could be more informative.

Conclusions: The lack of IRBP before eye opening prevents subsequent adjustments to achieve a normal eye size and response to form deprivation in the mouse eye. The absence of IRBP affects downstream mechanisms that might be expected to correct for the abnormally elongated eye and myopia of the IRBP KO mouse during emmetropization. Another explanation is that there are separate mechanisms altogether, and the mutation in IRBP has such a massive effect that the visually-driven pathways cannot compensate. There are more total TH-positive amacrine cells in the IRBP KO mouse retina than in the WT mouse retina. This may suggest that the lack of IRBP manifests problems that precede the use of the dopaminergic amacrine cells in emmetropization. Although there are subtle changes in retina morphology when the IRBP KO mouse retina is compared to the WT mouse retina, there were no major changes in the functional behavioral measure of visual acuity with OKT, which implies that optokinetic responses are robust and unaffected by severe myopic shifts. Ultimately, the experiments suggested that the abnormal increased eye elongation that starts at P7 in the IRBP KO mouse is unaffected by and precedes the processes of emmetropization.

The most interesting implication is that in myopia, ocular development may be generally accelerated. For whatever reason, by the time focus-dependent processes become possible, too much growth has already occurred. That is, there is a balance between the rate of growth and the rate of development of focus-dependent growth suppression. Possibly, myopic eyes simply develop too quickly before the onset of focus capabilities. This may be an imbalance, or

the timing is off, with growth coming too early and focus coming too late. Thus, it may be that the loss of IRBP simply allows too rapid growth due to too much free morphogen (which normally would be bound to IRBP) or too late an onset of focus capability, again, possibly due to too much free morphogen being accessible to cells when it ought to be sequestered by IRBP.

APPENDIX 1.

Figure 3B. Nasal-temporal length in WT and KO mice at ages P5 through P10. Figure 3C. Superior-Inferior length in WT and KO mice at ages P5 through P10. These panels indicate excessive equatorial growth of the eye on these two axes, in agreement with eye weight (Figure 2) and axial length data (Figure 3A). To access the data, click or select the words "Appendix 1."

APPENDIX 2.

Supporting figures for scleral and choroidal thickness by histological morphometry (Figures 4B-E). Slight thinning of layers is detectable at about P8 and older. To access the data, click or select the words "Appendix 2."

APPENDIX 3.

Figure 6A, Dopamine; Figure 6B, DOPAC; and Figure 6C DOPAC to dopamine ratio data from P7 to P60. These panels support normal levels of dopamine and DOPAC in the IRBP KO mouse with a very similar ratio of DOPAC to dopamine in the WT and KO mouse retinas. To access the data, click or select the words "Appendix 3."

ACKNOWLEDGMENTS

We are grateful for support provided by the Abraham J. & Phyllis Katz Foundation , NIH R01EY014026, R01EY021592, R01EY016470, VA RR&D C1924P I21RX001924, VA RR&D C9246C (Atlanta VA Center of Excellence in Vision and Neurocognitive Rehabilitation), P30EY006360, and an unrestricted grant to the Department of Ophthalmology at Emory University from Research to Prevent Blindness, Inc.

REFERENCES

1. Pfeffer B, Wiggert B, Lee L, Zonnenberg B, Newsome D, Chader G. The presence of a soluble interphotoreceptor retinol-binding protein (IRBP) in the retinal interphotoreceptor space. J Cell Physiol 1983; 117:333-41. [PMID: 6686234].
2. Baer CA, Van Niel EE, Cronk JW, Kinter MT, Sherman NE, Braiman MS, Gonzalez-Fernandez F. Arginine to glutamine substitutions in the fourth module of Xenopus interphotoreceptor retinoid-binding protein. Mol Vis 1998; 4:30-[PMID: 9873068].
3. Nickerson JM, Li GR, Lin ZY, Takizawa N, Si JS, Gross EA. Structure-function relationships in the four repeats of human interphotoreceptor retinoid-binding protein (IRBP). Mol Vis 1998; 4:33-[PMID: 9873071].
4. Rengarajan K, Pohl J, Nickerson J. Photoaffinity labeling of human IRBP with all-trans-retinoic acid. Biochem Biophys Res Commun 2001; 284:268-74. [PMID: 11394872].
5. Crouch RK, Hazard ES, Lind T, Wiggert B, Chader G, Corson DW. Interphotoreceptor retinoid-binding protein and alpha-tocopherol preserve the isomeric and oxidation state of retinol. Photochem Photobiol 1992; 56:251-5. [PMID: 1502268].
6. Loew A, Gonzalez-Fernandez F. Crystal structure of the functional unit of interphotoreceptor retinoid binding protein. Structure 2002; 10:43-9. [PMID: 11796109].
7. Lamb TD, Pugh EN. Dark adaptation and the retinoid cycle of vision. Prog Retin Eye Res 2004; 23:307-80. [PMID: 15177205].
8. Lamb TD, Pugh EN. Phototransduction, dark adaptation, and rhodopsin regeneration the proctor lecture. Investigative Ophthalmology &amp Visual Science 2006; 47:5138-52. .
9. Okajima TI, Pepperberg DR, Ripps H, Wiggert B, Chader GJ. Interphotoreceptor retinoid-binding protein promotes rhodopsin regeneration in toad photoreceptors. Proc Natl Acad Sci USA 1990; 87:6907-11. [PMID: 2118660].
10. Okajima TI, Pepperberg DR, Ripps H, Wiggert B, Chader GJ. Interphotoreceptor retinoid-binding protein: role in delivery of retinol to the pigment epithelium. Exp Eye Res 1989; 49:629-44. [PMID: 2509230].
11. Okajima TI, Wiggert B, Chader GJ, Pepperberg DR. Retinoid processing in retinal pigment epithelium of toad (Bufo marinus). J Biol Chem 1994; 269:21983-9. [PMID: 8071318].
12. Jones GJ, Crouch RK, Wiggert B, Cornwall MC, Chader GJ. Retinoid requirements for recovery of sensitivity after visual-pigment bleaching in isolated photoreceptors. Proc Natl Acad Sci USA 1989; 86:9606-10. [PMID: 2594788].
13. Jin J, Jones GJ, Cornwall MC. Movement of retinal along cone and rod photoreceptors. Vis Neurosci 1994; 11:389-99. [PMID: 8003460].
14. Jin M, Li S, Nusinowitz S, Lloyd M, Hu J, Radu RA, Bok D, Travis GH. The role of interphotoreceptor retinoid-binding protein on the translocation of visual retinoids and function of cone photoreceptors. J Neurosci 2009; 29:1486-95. [PMID: 19193895].
15. Parker RO, Fan J, Nickerson JM, Liou GI, Crouch RK. Normal cone function requires the interphotoreceptor retinoid binding protein. J Neurosci 2009; 29:4616-21. [PMID: 19357286].
16. Pitale PM, McKeown AS, Kraft TW. Role of Interphotoreceptor binding protein (IRBP) and Insulin-like Growth Factor-1 (IGF-1) in enhancing sensitivity of rod photoreceptors in

isolated mouse retina ARVO Annual Meeting; 2015 May 3-7; Seattle, (WA).

17. McKeown AS, Kraft TW. Adaptive potentiation in rod photoreceptors after light exposure. J Gen Physiol 2014; 143:733-43. [PMID: 24821966].

18. den Hollander A, McGee T, Ziviello C, Banfi S, Dryja T, Gonzalez-Fernandez F, Ghosh D, Berson E. A homozygous missense mutation in the IRBP gene (RBP3) associated with autosomal recessive retinitis pigmentosa. Investigative Ophthalmology &amp Visual Science 2008; 50:1864-72. .

19. Arno G, Hull S, Robson AG, Holder GE, Cheetham ME, Webster AR, Plagnol V, Moore AT. Lack of interphotoreceptor retinoid binding protein, caused by homozygous mutation of RBP3, is associated with high myopia and retinal dystrophy. Investigative Ophthalmology & Visual Science 2015.

20. Chen P, Miyake M, Fan Q, Liao J, Yamashiro K, Ikram MK, Chew M, Vithana EN, Khor C-C, Aung T, Tai E-S, Wong T-Y, Teo Y-Y, Yoshimura N, Saw SM, Cheng C-Y. CMPK1 and RBP3 are associated with corneal curvature in Asian populations. Hum Mol Genet 2014; [PMID: 24963161].

21. Liou GI, Fei Y, Peachey NS, Matragoon S, Wei S, Blaner WS, Wang Y, Liu C, Gottesman ME, Ripps H. Early onset photoreceptor abnormalities induced by targeted disruption of the interphotoreceptor retinoid-binding protein gene. J Neurosci 1998; 18:4511-20. [PMID: 9614228].

22. Wisard J, Faulkner A, Chrenek MA, Waxweiler T, Waxweiler W, Donmoyer C, Liou GI, Craft CM, Schmid GF, Boatright JH, Pardue MT, Nickerson JM. Exaggerated eye growth in IRBP-deficient mice in early development. Investigative Ophthalmology &amp Visual Science 2011; 52:5804-11. .

23. Ripps H, Peachey NS, Xu X, Nozell SE, Smith SB, Liou GI. The rhodopsin cycle is preserved in IRBP "knockout" mice despite abnormalities in retinal structure and function. Vis Neurosci 2000; 17:97-105. [PMID: 10750831].

24. Troilo D, Wallman J. The regulation of eye growth and refractive state: an experimental study of emmetropization. Vision Res 1991; 31:1237-50. [PMID: 1891815].

25. Wallman J. Retinal influences on sclera underlie visual deprivation myopia. Ciba Found Symp 1990; 155:126-34. , discussion 35–41.. [PMID: 2088673].

26. Smith EL, Ramamirtham R, Qiao-Grider Y, Hung L-F, Huang J, Kee C-S, Coats D, Paysse E. Effects of foveal ablation on emmetropization and form-deprivation myopia. Investigative Ophthalmology &amp Visual Science 2007; 48:3914-22. .

27. Smith EL, Hung L-F, Huang J. Relative peripheral hyperopic defocus alters central refractive development in infant monkeys. Vision Res 2009; 49:2386-92. [PMID: 19632261].

28. Smith EL, Huang J, Hung L-F, Blasdel TL, Humbird TL, Bockhorst KH. Hemiretinal form deprivation: evidence for local control of eye growth and refractive development in infant monkeys. Investigative Ophthalmology &amp Visual Science 2009; 50:5057-69. .

29. Guo L, Frost MR, He L, Siegwart JT, Norton TT. Gene expression signatures in tree shrew sclera in response to three myopiagenic conditions. Investigative Ophthalmology &amp Visual Science 2013; 54:6806-19. .

30. Stone RA, Lin T, Laties AM, Iuvone PM. Retinal dopamine and form-deprivation myopia. Proc Natl Acad Sci USA 1989; 86:704-6. [PMID: 2911600].

31. Feldkaemper M, Schaeffel F. An updated view on the role of dopamine in myopia. Exp Eye Res 2013; [PMID: 23434455].

32. McFadden SA, Howlett MHC, Mertz JR, Wallman J. Acute effects of dietary retinoic acid on ocular components in the growing chick. Exp Eye Res 2006; 83:949-61. [PMID: 16797531].

33. Mertz JR, Wallman J. Choroidal retinoic acid synthesis: a possible mediator between refractive error and compensatory eye growth. Exp Eye Res 2000; 70:519-27. [PMID: 10866000].

34. Wildsoet CF, Pettigrew JD. Kainic acid-induced eye enlargement in chickens: differential effects on anterior and posterior segments. Investigative Ophthalmology &amp Visual Science 1988; 29:311-9. .

35. Wildsoet C. Neural pathways subserving negative lens-induced emmetropization in chicks–insights from selective lesions of the optic nerve and ciliary nerve. Curr Eye Res 2003; 27:371-85. [PMID: 14704921].

36. Rymer J, Wildsoet CF. The role of the retinal pigment epithelium in eye growth regulation and myopia: a review. Vis Neurosci 2005; 22:251-61. [PMID: 16079001].

37. Fishman GA, Anderson RJ, Lourenco P. Prevalence of posterior subcapsular lens opacities in patients with retinitis pigmentosa. Br J Ophthalmol 1985; 69:263-6. [PMID: 3994942].

38. Heckenlively J. The frequency of posterior subcapsular cataract in the hereditary retinal degenerations. Am J Ophthalmol 1982; 93:733-8. [PMID: 7091261].

39. Joy A, Al-Ghoul KJ. Basal membrane complex architecture is disrupted during posterior subcapsular cataract formation in Royal College of Surgeons rats. Mol Vis 2014; 20:1777-95. [PMID: 25593506].

40. Mattapallil MJ, Wawrousek EF, Chan C-C, Zhao H, Roychoudhury J, Ferguson TA, Caspi RR. The rd8 mutation of the Crb1 gene is present in vendor lines of C57BL/6N mice and embryonic stem cells, and confounds ocular induced mutant phenotypes. Investigative Ophthalmology & Visual Science 2012.

41. Johnson CJ, Berglin L, Chrenek MA, Redmond TM, Boatright JH, Nickerson JM. Technical brief: subretinal injection and electroporation into adult mouse eyes. Mol Vis 2008; 14:2211-26. [PMID: 19057658].

42. Muranov K, Poliansky N, Winkler R, Rieger G, Schmut O, Horwath-Winter J. Protection by iodide of lens from selenite-induced cataract. Graefe's archive for clinical and experimental ophthalmology = Albrecht Von Graefes Arch Klin Exp Ophthalmol 2004; 242:146-51. .

43. Mills RA, Jones DB, Winkler CR, Wallace GW, Wilhelmus KR. Topical FK-506 prevents experimental corneal allograft rejection. Cornea 1995; 14:157-60. [PMID: 7538061].

44. Dysli C, Enzmann V, Sznitman R, Zinkernagel MS. Quantitative Analysis of Mouse Retinal Layers Using Automated Segmentation of Spectral Domain Optical Coherence Tomography Images. Transl Vis Sci Technol 2015; 4:9-[PMID: 26336634].

45. Berger A, Cavallero S, Dominguez E, Barbe P, Simonutti M, Sahel J-A, Sennlaub F, Raoul W, Paques M, Bemelmans A-P. Spectral-domain optical coherence tomography of the rodent eye: highlighting layers of the outer retina using signal averaging and comparison with histology. PLoS One 2014; 9:e96494-[PMID: 24788712].

46. Chakraborty R, Park HN, Aung MH, Tan CC, Sidhu CS, Iuvone PM, Pardue MT. Comparison of refractive development and retinal dopamine in OFF pathway mutant and C57BL/6J wild-type mice. Mol Vis 2014; 20:1318-27. [PMID: 25352740].

47. Wisard J, Chrenek MA, Wright C, Dalal N, Pardue MT, Boatright JH, Nickerson JM. Non-contact measurement of linear external dimensions of the mouse eye. J Neurosci Methods 2010; 187:156-66. [PMID: 20067806].

48. Boatright JH, Dalal N, Chrenek MA, Gardner C, Ziesel A, Jiang Y, Grossniklaus HE, Nickerson JM. Methodologies for analysis of patterning in the mouse RPE sheet. Mol Vis 2015; 21:40-60. [PMID: 25593512].

49. Chrenek MA, Dalal N, Gardner C, Grossniklaus H, Jiang Y, Boatright JH, Nickerson JM. Analysis of the RPE sheet in the rd10 retinal degeneration model. Adv Exp Med Biol 2012; 723:641-7. [PMID: 22183388].

50. Bhatia SK, Rashid A, Chrenek MA, Zhang Q, Bruce BB, Klein M, Boatright JH, Jiang Y, Grossniklaus HE, Nickerson JM. Analysis of RPE morphometry in human eyes. Mol Vis 2016; 22:898-916. [PMID: 27555739].

51. Iuvone PM, Boatright JH, Bloom MM. Dopamine mediates the light-evoked suppression of serotonin N-acetyltransferase activity in retina. Brain Res 1987; 418:314-24. [PMID: 2445415].

52. Boatright JH, Hoel MJ, Iuvone PM. Stimulation of endogenous dopamine release and metabolism in amphibian retina by light- and K+-evoked depolarization. Brain Res 1989; 482:164-8. [PMID: 2706474].

53. Park HN, Jabbar SB, Tan CC, Sidhu CS, Abey J, Aseem F, Schmid G, Iuvone PM, Pardue MT. Visually-driven ocular growth in mice requires functional rod photoreceptors. Investigative Ophthalmology &amp Visual Science 2014; 55:6272-9. .

54. Faulkner AE, Kim MK, Iuvone PM, Pardue MT. Head-mounted goggles for murine form deprivation myopia. J Neurosci Methods 2007; 161:96-100. [PMID: 17126909].

55. Schaeffel F, Farkas L, Howland HC. Infrared photoretinoscope. Appl Opt 1987; 26:1505-9. [PMID: 20454351].

56. Faulkner A, Kim M, Iuvone P, Pardue M. Head-mounted goggles for murine form deprivation myopia. J Neurosci Methods 2007; [PMID: 17126909].

57. Douglas R, Alam N, Silver B. Independent visual threshold measurements in the two eyes of freely moving rats and mice using a virtual-reality optokinetic system. Visual … 2005.

58. Wright CB, Chrenek MA, Foster SL, Duncan T, Redmond TM, Pardue MT, Boatright JH, Nickerson JM. Complementation test of Rpe65 knockout and tvrm148. Investigative Ophthalmology & Visual Science 2013.

59. Wright CB, Chrenek MA, Feng W, Getz S, Duncan T, Pardue MT, Feng Y, Redmond TM, Boatright JH, Nickerson JM. The Rpe65rd12 allele exerts a semidominant effecton on vision in mice. Investigative Ophthalmology & Visual Science 2014.

60. Pardue MT, Faulkner AE, Fernandes A, Yin H, Schaeffel F, Williams RW, Pozdeyev N, Iuvone PM. High susceptibility to experimental myopia in a mouse model with a retinal on pathway defect. Investigative Ophthalmology &amp Visual Science 2008; 49:706-12. .

61. Schaeffel F, Burkhardt E, Howland HC, Williams RW. Measurement of refractive state and deprivation myopia in two strains of mice. Optom Vis Sci 2004; 81:99-110. [PMID: 15127929].

62. Schmucker C, Schaeffel F. In vivo biometry in the mouse eye with low coherence interferometry. Vision Res 2004; 44:2445-56. [PMID: 15358080].

63. Nickerson JM, Borst DE, Redmond TM, Si JS, Toffenetti J, Chader GJ. The molecular biology of IRBP: application to problems of uveitis, protein chemistry, and evolution. Prog Clin Biol Res 1991; 362:139-61. [PMID: 2003124].

64. Inouye LN, Albini A, Chader GJ, Redmond TM, Nickerson JM. mRNA for interphotoreceptor retinoid-binding protein (IRBP): distribution and size diversity in vertebrate species. Exp Eye Res 1989; 49:171-80. [PMID: 2767165].

65. Liou GI, Wang M, Matragoon S. Precocious IRBP gene expression during mouse development. Investigative Ophthalmology &amp Visual Science 1994; 35:1083-8. .

66. Carter-Dawson L, Alvarez RA, Fong SL, Liou GI, Sperling HG, Bridges CD. Rhodopsin, 11-cis vitamin A, and interstitial retinol-binding protein (IRBP) during retinal development in normal and rd mutant mice. Dev Biol 1986; 116:431-8. [PMID: 3732615].

67. Aung MH, Kim MK, Olson DE, Thule PM, Pardue MT. Early visual deficits in streptozotocin-induced diabetic long evans rats. Investigative Ophthalmology &amp Visual Science 2013; 54:1370-7. .

68. Schmucker C, Schaeffel F. A paraxial schematic eye model for the growing C57BL/6 mouse. Vision Res 2004; 44:1857-67. [PMID: 15145680].

69. Cazin L, Precht W, Lannou J. Pathways mediating optokinetic responses of vestibular nucleus neurons in the rat. Pflugers Arch 1980; 384:19-29. [PMID: 6247696].

70. Brand C, Burkhardt E, Schaeffel F, Choi JW, Feldkaemper MP. Regulation of Egr-1, VIP, and Shh mRNA and Egr-1 protein in the mouse retina by light and image quality. Mol Vis 2005; 11:309-20. [PMID: 15889015].

Articles are provided courtesy of Emory University and the Zhongshan Ophthalmic Center, Sun Yat-sen University, P.R. China. The print version of this article was created on 27 October 2016. This reflects all typographical corrections and errata to the article through that date. Details of any changes may be found in the online version of the article.